Rayleigh instability of confined vortex droplets in critical superconductors

I. Lukyanchuk[1], V. M. Vinokur[2], A. Rydh[3], R. Xie[2], M. Milošević[4], U. Welp[2], M. Zach[2], Z. L. Xiao[2], G. W. Crabtree[2], S. Bending[5], F. Peeters[4], and W. K. Kwok[2]

[1]*Laboratory of Condensed Matter Physics, University of Picardie, Amiens, France*
[2]*Materials Science Division, Argonne National Laboratory, 9700 South Cass Avenue, Argonne, IL 60439, USA*
[3]*Department of Physics: Stockholm University, Albanova University Center, SE-10691 Stockholm, Sweden*
[4]*Department of Physics, University of Antwerpen, Groenenborgerlaan 171, B-2020 Antwerpen, Belgium*
[5]*Department of Physics, University of Bath, Claverton Down, Bath BA2 7AY, Umted Kingdom*

Depending on the Ginzburg-Landau material parameter κ, superconductors can either be fully diamagnetic if $\kappa < 1/\sqrt{2}$ (type I superconductors) or accommodate magnetic field in the form of Abrikosov vortices if $\kappa > 1/\sqrt{2}$ (type II superconductors).[1,2] At Bogomolny critical point, $\kappa = \kappa_c = 1/\sqrt{2}$, a state, infinitely degenerated with respect to vortex spatial configurations, arises.[3,4] While conventional type I and type II superconductors are investigated in depth, a thorough understanding of magnetic behaviour in the near-Bogomolny critical regime at $\kappa \sim \kappa_c$ is still lacking. Here we report that in restricted systems the critical regime expands over a finite interval of κ forming *critical superconducting state*. We show that in this state, in a sample with dimensions comparable with the vortex core size, vortices merge into a multi-quanta droplet, which undergoes Rayleigh instability[5] upon increasing κ and decays by emitting single vortices. Superconducting vortices materialize Nielsen-Olesen singular solutions of the Abelian Higgs model pervasive in phenomena ranging from quantum electrodynamics to cosmology.[6,7,8,9] Our work, revealing transient dynamics of Abrikosov-Nielsen-Olesen vortices in systems with boundaries, promises access to novel effects in quantum field theory via bench-top laboratory experiments.

The evolution of magnetic properties of an infinite superconductor when crossing κ_c is shown in Fig. 1. Type I superconductors with $\kappa < \kappa_c$ expel magnetic field *H* until it reaches a critical field H_c beyond which superconductivity is destroyed (Fig. 1 b,e). In type II superconductors with $\kappa > \kappa_c$, superconductivity extends into a wider region, $H_{c1} < H < H_{c2}$, where magnetic field penetrates the sample in the form of Abrikosov vortices, tiny filaments of the normal phase surrounded by encircling supercurrents (Fig. 1 a,d), each carrying a quantum magnetic flux $\Phi_0 = \pi\hbar/ce$.

Finite-size systems acquire new features enriching their phase diagram. Most importantly, type I superconductors fall into an *intermediate state*, comprising alternating domains of normal and superconducting phases with the period $d \simeq 10\sqrt{D\xi}$ for $H \simeq 0.5H_c$,[10] where ξ is the coherence length and *D* is the sample thickness. The intermediate state forms in the interval $(1-n)H_c < H < H_c$ (n < 1 is the shape-dependent demagnetization factor) triggered by the local magnetic field near the edges of the sample exceeding the critical value H_c and locally destroying superconductivity (Fig. 1c, f). In type II superconductors, nucleation of superconductivity occurs first near the sample boundary at a specific surface critical field $H_{c3} > H_{c2}$. In type I superconductors H_{c3} can exceed H_c if $\kappa \lesssim \kappa_c$, as shown in Fig. 1b,e.

Near kappa-induced criticality, with domains containing only a few flux quanta, the intermediate state is unstable towards breaking into an Abrikosov lattice and transient effects become important. To analyze transient behavior, we consider a sample with $\kappa \lesssim \kappa_c$ containing a single domain or droplet of the normal phase, i.e. a sample with the lateral size *L* comparable with the period *d* of the domain structure. This droplet is nothing but a giant vortex with a normal core comprising several flux quanta.[11] Its critical fission occurs via splitting an *N*-quanta-droplet (*Nq*-droplet) into a $(N-1)q$-droplet and a single *1q* vortex moving away, see Fig. 2. To calculate the energy difference between the *Nq*-droplet and the configuration consisting of the residual $(N-1)q$-droplet and the separated vortex, we construct a perturbation theory in the vicinity of the Bogomolny point over the small parameter $\gamma = \kappa^2 - \kappa_c^2$ [see Supplementary Information (SI)] and identify three contributions to the interaction energy, see Fig. 2c:

$$U(l) = U_e(l) + U_i(l) + U_c(l), \tag{1}$$

where *l* is the distance between the vortex and the droplet. The intrinsic interaction energy of the *(N-1)q*-droplet with the separated vortex calculated in,[12] see also SI and,[13] is

$$U_e(l) = -\gamma\, \frac{\alpha}{4\sqrt{N}} \frac{D}{\lambda} H_c^2\, \lambda\, l^2, \qquad \alpha \simeq 0.3\,, \tag{2}$$

where λ is the London electromagnetic screening length. This term yields attraction at γ <0 as expected. Magnetostatic repulsion energy due to stray fields generated by vortices near the sample surface, is

$$U_i(l) = -2\,\zeta(N)\, H_c^2\, \lambda\, l^2, \quad \zeta(N) \simeq 0.04\sqrt{N}. \tag{3}$$

Finally, the confinement energy due to interaction of the external field *H* with the vortex, holding the droplet together is:

$$U_c(l) = 2\,\eta\, \frac{H}{H_c} \frac{\lambda}{L} H_c^2\, \lambda\, l^2, \qquad \eta \simeq 0.52\,. \tag{4}$$

As follows from Eq. (4), decreasing the field reduces the confinement strengths. At some threshold field, the repulsive forces begin to dominate and a single vortex splits from the

droplet. Upon further decreasing the field, individual vortices sequentially detach from the droplet and escape from the sample. This disintegration mechanism is analogous to the instability introduced by Lord Rayleigh[5] in 1882 leading to fragmentation of charged liquid droplets due to the competition between long-range Coulomb repulsion forces and a short-range molecular attraction.

The threshold field $H_{\rm inst}(N)$ at which the Nq-droplet becomes unstable is determined from the instability point when the energy $U(l)$ changes its curvature and transforms from a convex function to a concave one, and Eqs. (1) – (4), yield:

$$H_{inst}(N) = \frac{L}{\lambda_0}\left[\frac{\zeta(N)}{\eta}t^{1/2} + \gamma\frac{\alpha}{8\eta\sqrt{N}}\frac{D}{\lambda_0}t\right]H_c\ . \qquad (5)$$

Direct disintegration of an Nq-droplet into N single vortices requires surmounting a higher confinement energy barrier than one-by-one vortex decoupling.

The Rayleigh instability can be observed if the field $H_{inst}(N)$ falls into the region of the existence of the vortex droplet. On the descending field branch, vortex droplet appears as a residual of the normal state in the finite sample below the surface critical field $H_{c3} = 2.39\kappa H_c$. Alternatively, on the ascending branch, the droplet can form as a result of the field penetration in a Meissner state. The threshold is defined by the condition that the external field at the sample edges, $H/(1-n)$, exceeds the field of first penetration into an *infinite* sample, $H_p \simeq \frac{1}{2^{1/4}\kappa^{1/2}}\frac{1+5.44\kappa}{1+4.78\kappa}H_c$,[14] which gives the superheating field $H_{sh} = (1-n)H_p$ for the lower bound of field penetration into a *finite* superconducting sample.

Criticality can be tuned by temperature variation of $\kappa(T) = \lambda(T)/\xi(T)$. In a Pb superconductor $\kappa(T)$ changes from $\mathrm{c}(0) \approx 0.68$ at $T = 0$, which is slightly less than κ_c, to $\kappa \simeq 0.38$ at $T = T_c(7.2\ K)$ and is well described by the phenomenological formula $\kappa(T) \simeq \kappa(0)/(1 + T^2/T_c^2)$,[15] see Fig. 3b. Therefore, micron-sized samples of Pb, an exemplary type I superconductor, offer a natural laboratory to study vortex droplet fission. We selected a triangular shaped Pb meso-crystal with lateral side dimensions of ~*2.2* μm, thickness of ~*0.7*μm, and critical temperature $T_c = 7.18\ K$ shown in the lower inset of Fig. 3a. The measurements on the crystal were done using a two-dimensional electron gas (2DEG) ballistic Hall micro-probe array magnetometer[16,17] (see Fig. 3a lower inset). The temperature variation of κ gives rise to the phase diagram of Pb shown in Fig. 3c. The temperature dependence for H_c is standard, $H_c(T) = H_c(0)[1 - (T/T_c)^2]$, with $\mu_0 H_c(0) \approx 78$ mT .[18] The critical fields H_{sh} and H_{c3} are expressed through H_c as given above with the best-fit value n = 0.37. The curves for H_c, H_{sh} and H_{c3} cross pair-wise near approximately $T_x \simeq 6.3\ K$. The dotted lines show the instability field $H_{inst}(N)$ for various N calculated from equation (5). We further focus on the temperature region $T_x < T < T_c$, which is the most favorable for the experimental observation of Rayleigh instability of the vortex droplet. At $T < T_x$ the lines $H_{inst}(N)$ for large N fall out from the range of existence of superconductivity, implying that there the droplet may become unstable with respect to splitting into single vortices. Our 3D numerical simulations, done using the phenomenologically adapted Ginzburg-Landau theory to account for the correct temperature dependence of κ and H_c,[19] show the intermediate regime with a mixture of droplet and one-quanta vortices, see Fig. 4. Note that in the temperature range $T_x < T < T_c$ where $H_{c3} < H_c < H_{sh}$, the droplet can form only in the descending field regime, since in ascending field the sample remains in the Meissner state until the field reaches H_{sh} at which superconductivity vanishes.

The temperature dependencies of H_c, H_{sh} and H_{c3} displayed in Fig. 3c are in a good agreement with those of Fig. 3a obtained experimentally. The data were extracted from field dependent magnetization curves as shown in the upper inset to Fig. 3a. From H_{sh} and H_c one obtains the temperature dependence of the Ginzburg-Landau parameter $\kappa(T)$ through H_p. The temperature dependence of the Ginzburg-Landau parameter $\kappa(T) = \lambda(T)/\xi(T)$ corresponds to the bulk behavior, shown in Fig. 3b. Together with $H_c(T)$ this gives a penetration $\lambda(T) \approx \lambda(0)/[1 - (T/T_c)^2]$ with $\lambda(0) \approx 41$ nm and a zero temperature coherence length $\xi(0)\approx 66$ nm. To see the droplet fission, we use the individual vortex observation technique, analogous to that used in[16] for observation of entrance and exit of individual vortices in small type II superconductors. The $M(H)$ dependencies at $T = 2$K and at $T = 6.7$K shown in insets of Fig. 3b and Fig. 3d have a different character, the difference stemming from the temperature dependence of $\kappa(T)$.

At $T = 2$ K, where $\kappa \simeq 0.6 - 0.7$ and is slightly less than κ_c, the lower inset of Fig. 3b delineates the mixed-state-like behavior of $M(H)$ in which the individual vortices are stabilized by the repulsion due to the stray field. First, upon increasing the applied field to $H_{sh} \simeq 51$ mT from the zero-field-cooled state, the absolute value of the magnetization grows proportionally to H due to Meissner screening. Beyond H_{sh}, the magnetic flux starts to penetrate the sample and the magnetization decreases smoothly. An extrapolation of the linear drop of the absolute value of $M(H)$ to zero agrees with the bulk value $H_c \simeq 71$ mT, but the diamagnetic signature of superconductivity disappears only at $H = H_{c3} \simeq 96$ mT (see Fig. 3a,b). At the reversing branch, the onset of the transition is observed at $H \approx H_{c3}$ but the magnetization remains close to zero, as long as the magnetic flux can freely leave the sample. Upon further change of H, the magnetization becomes modulated by a saw-like structure, which reflects the effect of pinning that traps vortices within the sample. The drops in $M(H)$ dependence correspond to the one-by-one escape of vortices from the sample, similar to what is observed in[16,20]. Upon switching the sign of the field, vortices leave the sample, which finally falls into the Meissner state and the process repeats itself cyclically.

The full $M(H)$ curve at $T = 6.7$ K, shown in the inset of Fig. 3d, is exemplary for the single droplet regime at $T_x < T < T_c$ where H_{c3}, $H_c < H_{sh}$ are close to each other and where by tuning the field we can control the vortex droplet fission. An expanded view of one quadrant of the data is shown in Fig. 5 for T=6.7 K and 7.0 K. On the ascending field at T = 6.7 K, the Meissner state is maintained up to H_{sh}. At $H = H_{sh}$ the magnetization abruptly drops to zero. Moving from high field along the descending branch, one sees that superconductivity emerges at $H_{c3}(T)$, but the system falls into a vortex droplet state.

After formation of superconductivity, $M(H)$ at the descending branch follows the envelope shape $4\pi M = (n^{-1} - 1)(H - H_c)$ modulated by the single quantum jumps due to one-by-one escape of vortices from the sample. Deviation from this dependence starts at $H = 0.85H_c$ marking the transition of the intermediate state to the metastable regime of the vortex droplet containing N=5 bounded vortices. Upon further field reduction, the disintegration of the droplet follows the scenario of instability, governed by Eq. (5). We marked experimentally observed values of $H_{inst}(N)$ for N=5,4,3 and 2 on the theoretical phase diagram Fig. 3d by solid red dots. The data show a perfect agreement with theoretical predictions. The final two-quanta jump corresponds to disappearance of the last 2-quanta droplet: the last 2q vortex droplet splits symmetrically so that both vortices leave the sample simultaneously. A similar behavior is observed in the T = 7.0 K data (Fig. 5b), where the maximum quantum number is N = 3.

Besides, near T_c the coherence and screening lengths become comparable to the size of the sample, and the proposed theory applies only marginally. Thus, while, in general, the observations are consistent with the theoretical phase diagram of Fig. 3c,d, the experimental points appear slightly off the theoretical instability curves.

Methods summary

Micron-sized lead superconducting crystals were grown on a highly oriented pyrolytic graphite (HOPG) substrate syntheszied via an electrochemical process, which we developed earlier.[21] By carefully selecting the electrodeposition parameters, we can grow a plethora of 3D-shaped mesoscopic Pb superconductors with various geometries such as pyramids, pentagons, needles and brushes.

References

[1] Ginzburg, V. L. & Landau, L. D., On the theory of superconductivity, *Zh. Eksp. Teor. Fiz.* **20**, 1064-1082 (1950).

[2] Abrikosov, A. A. Magnetic properties of superconductors of the second group, *Zh. Éksp. Teor. Fiz*. **32**, 1442-1452 (1957) [*Sov. Phys. JETP* **5**, 1174-1182 (1957)].

[3] Bogomolnyi, E. B. The stability of classical solutions. *Yad. Fiz*. **24**, 861-870 (1976) [*Sov. J. Nucl. Phys*. **24**, 449-454 (1976)].

[4] Bogomolnyi, E. B. & Vainstein, A. I., Stability of strings in gauge Abelian theory, *Yad. Fiz*. **23**, 1111 -1114 (1976) [*Sov. J. Nucl. Phys*. **23**, 588-591 (1976)].

[5] Rayleigh, Lord, FRS. On the equilibrium of liquid conducting masses charged with electricity, *Philosophical Magazine*, Series 5, 14:87 184–186 (1882).

[6] Nielsen H. B. & Olesen P., Vortex-line models for dual strings. Nuclear Physics B **61**, 45–61 (1973).

[7] Bradlow, S., Vortices in holomorphic line bundles over closed Kahler manifolds, *Commun. Math. Phys*. **135**, 1–17 (1990).

[8] Gustafson, S., Sigal, I. M., & Tzaneteas, T., Statics and dynamics of magnetic vortices and of Nielsen–Olesen (Nambu) strings, J. Math. Phys. 51, 015217 (2010).

[9] Witten, E., From superconductors and four-manifolds to weak interactions, Bull. Amer. Math. Soc. **44** 361-391(2007).

[10] Landau, L. D. & Lifshitz, E. M., *Electrodynamics of Continuous Media*, (Elsevier, New York, 1985).

[11] Cren, T., Serrier-Garcia, L., Debontridder, F. & Roditchev, D., *Vortex Fusion and Giant Vortex States in Confined Superconducting Condensates*, *Phys. Rev. Lett*. **107**, 097202 (2011).

[12] Luk'yanchuk, I., Theory of superconductors with κ close to $1/\sqrt{2}$, *Phys. Rev*. B **63**, 174504 (2001).

[13] Mohamed, F., Troyer, M., Blatter, G. & Luk'yanchuk, I., Interaction of vortices in superconductors with κ close to $1/\sqrt{2}$, *Phys. Rev*. B **65**, 224504 (2002).

[14] Dolgert, A. J., Di Bartolo, S. J. & Dorsey A. T., Superheating fields of superconductors: Asymptotic analysis and numerical results, *Phys. Rev*. B **53**, 5650-5660 (1996).

[15] Cody, G. D. & Miller, R. E., Magnetic Transitions of Superconducting Thin Films and Foils. I. Lead. *Phys. Rev*. **173**, 481-493 (1968).

[16] Geim, A. K., Grigorieva, I. V., Dubonos, S. V., Lok J. G. S., Maan J. C., Filippov A. E. & Peeters F. M. Phase transitions in individual sub-micrometre superconductors, *Nature* **390**, 259-262 (1997)

[17] Rydh, A., Xie, R., Zach, M., Welp, U., Kwok, W. K., Crabtree, G.W., Bending, S., Milosevic, M.V. & Peeters, F.M. Magnetization of a few-fluxoid lead crystal, *Physica C* **460**, 793-794 (2007).

[18] Rose-Innes, A. C. & Rhoderick, R. H., *Introduction to Superconductivity* (Pergamon Press, Oxford, 1969).

[19] Müller, A., Milošević, M. V., Dale, S. E. C., Engbarth, M. A., & Bending, S. J., Magnetization Measurements and Ginzburg-Landau Simulations of Micron-Size β-Tin Samples: Evidence for an Unusual Critical Behavior of Mesoscopic Type-I Superconductors, *Phys. Rev. Lett*. **109**, 197003 (2012).

[20] Geim, A. K., Dubonos, S. V., Palacios, J. J., Grigorieva, I. V., Henini, M. & Schermer, J. J. Fine Structure in Magnetization of Individual Fluxoid States, *Phys. Rev. Lett*. **85**, 1528-1531 (2000).

[21] Xiao, Z.-L., Han C. Y., Kwok W.-K., Wang, H.-H. Welp, U., Wang, J. & Crabtree, G. W., Tuning the architecture of mesostructures by electrodeposition, *J. Am. Chem. Soc*. **126**, 2316-2317 (2004).

Acknowledgments: We would like to thank N. Nekrasov for illuminating discussions. The work was supported by the U.S. Department of Energy, Office of Science Materials Sciences and Engineering Division (VV,WK,UW,RX,MZ,ZX,GC), by FP7-IRSES-SIMTECH and ITN-NOTEDEV programs (IL), and by Flemish Science Foundation (FWO-Vlaanderen) (MM, FP).

Author contributions: IL, VV, WK and UW conceived the work, IL and VV carried out calculations and analyzed the data, MZ and ZX grew the samples, AR, RX, UW and WK carried out the experiment, SB provided the Hall sensor, MM and FP performed numerical simulations, IL and VV wrote the manuscript, AR, UW, MM, GC, SB, FP, and WK discussed the results and contributed to writing the manuscript.

Competing Interests. The authors declare that they have no competing financial interests.

Correspondence Correspondence and requests for materials should be addressed to Igor Lukyanchuk (e-mail: lukyanc@ferroix.net).

Figure captions

Figure 1. Superconducting phase diagrams and corresponding magnetization curves. Top panel: phase diagrams and relevant critical fields for (a) type II, (b) critical, (c) type I, and (d) type I finite-size superconductors. Bottom panel, the corresponding *M(H)* dependencies. Note that $H_{c3} > H_c$ holds only as long as > 0.42 .

Figure 2. Droplet fission. Top panels: Distribution of the magnetic flux in the (a) Meissner state, (b) vortex droplet state showing the calculated stray fields and (c) sketch of the vortex interaction forces (F_e, F_c, and F_i) corresponding to the interaction energies (U_e, U_c and U_i) between the droplet and a separated single vortex. Bottom panels: (d) –(f) Sequential dynamics of the droplet fission process showing the calculated stray fields.

Figure 3. Experimantal phase diagrams. (a) Experimental phase diagram of the meso-Pb crystal. (top inset) *M(H)* at T=0.36K demonstrating how H_{sh}, H_{c3} and H_c were obtained experimentally. (bottom inset) experimental set-up of the crystal and the Hall probe array. (b) The $\kappa(T)$ dependence of Pb (adopted from[15]). (c) Theoretical temperature dependencies of H_c, H_{c3} and H_{sh}. (d) expanded interval $T_x<T<T_c$. Numbered dotted lines show the calculated locus of instabilities with respect to $N \rightarrow N\text{-}1$ vortex droplet fission. Red dots show the corresponding instabilities at T=6.7K and at T=7.0K, associated with the data in Fig. 5. (Inset to b) shows the experimental *M(H)* dependencies in the diluted vortex gas regime at T=2K and (Inset to d) in the metastable vortex-droplet fission regime at T=6.7K.

Figure 4. Exemplary vortex configurations in the critical region. Evolution of the ground state vortex structures upon decreasing magnetic field in a mesoscale triangular superconducting Pb prism at $\kappa \sim \kappa_c$ in the extended critical region where vortex droplet can coexist with separate vortices. This particular simulation is performed for T=5.5K, and parameters of the Pb sample T_c=7.2K, $\xi(0)$=66nm and $\lambda(0)$=45nm, with two-fluid model temperature dependencies [19].

Figure 5. Magnetization curves displaying vortex droplet fission. Experimental *M(H)* curves at (a) 6.7 K and (b) 7.0 K. The applied magnetic field is normalized by $H_c(T) = H_c(0)[1 - (T/T_c)^2]$, with $H_c(0) = 78$ mT and $T_c = 7.18$ K. On increasing field (red curves) the Meissner state ($N = 0$) survives up to $H_c \simeq H_{sh}$. On decreasing field (blue curves), the Nq-vortex droplet undergoes sequential Rayleigh decay (black arrows). The green curves show the full stability ranges of the droplet states, obtained by reversing the field sweep direction.

Figure 1

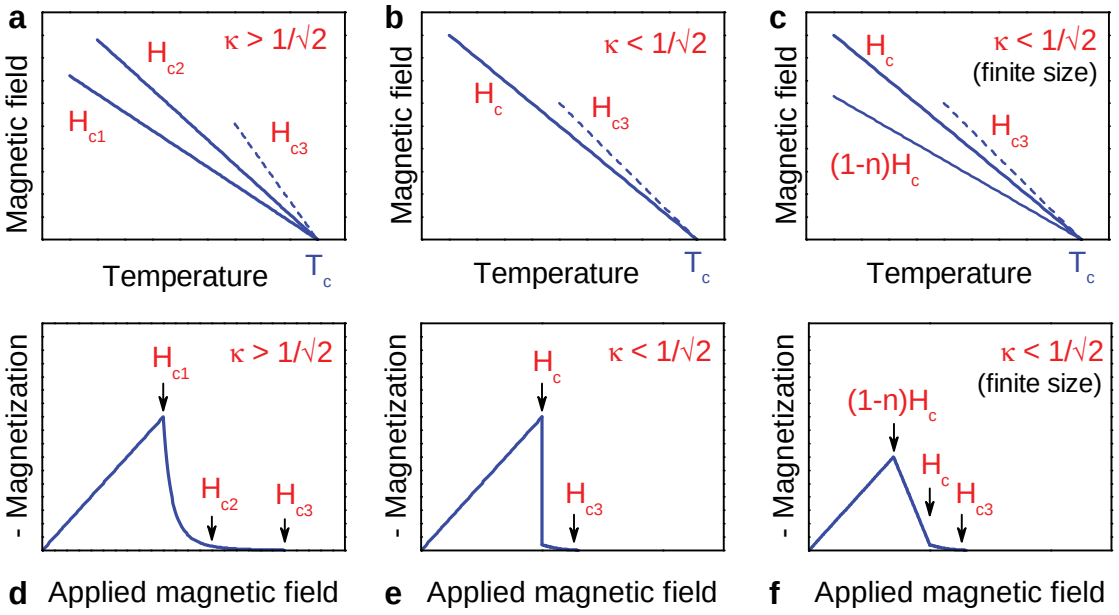
a
Magnetic field
Temperature
T_c
H_{c2}
H_{c1}
H_{c3}
$\kappa > 1/\sqrt{2}$
b
Magnetic field
Temperature
T_c
H_c
H_{c3}
$\kappa < 1/\sqrt{2}$
c
Magnetic field
Temperature
T_c
H_c
H_{c3}
$(1-n)H_c$
$\kappa < 1/\sqrt{2}$
(finite size)
- Magnetization
H_{c1}
H_{c2}
H_{c3}
$\kappa > 1/\sqrt{2}$
d Applied magnetic field
- Magnetization
H_c
H_{c3}
$\kappa < 1/\sqrt{2}$
e Applied magnetic field
- Magnetization
$(1-n)H_c$
H_c
H_{c3}
$\kappa < 1/\sqrt{2}$
(finite size)
f Applied magnetic field

Figure 2

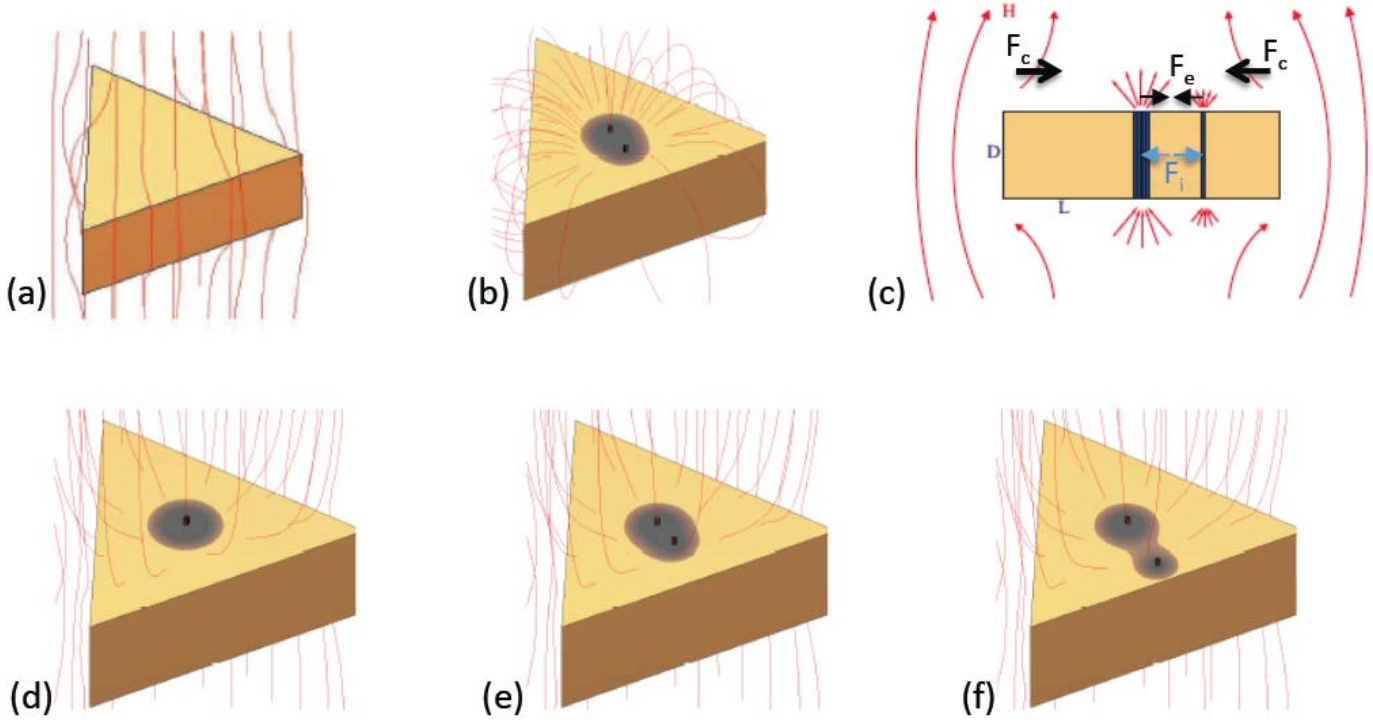

Figure 3

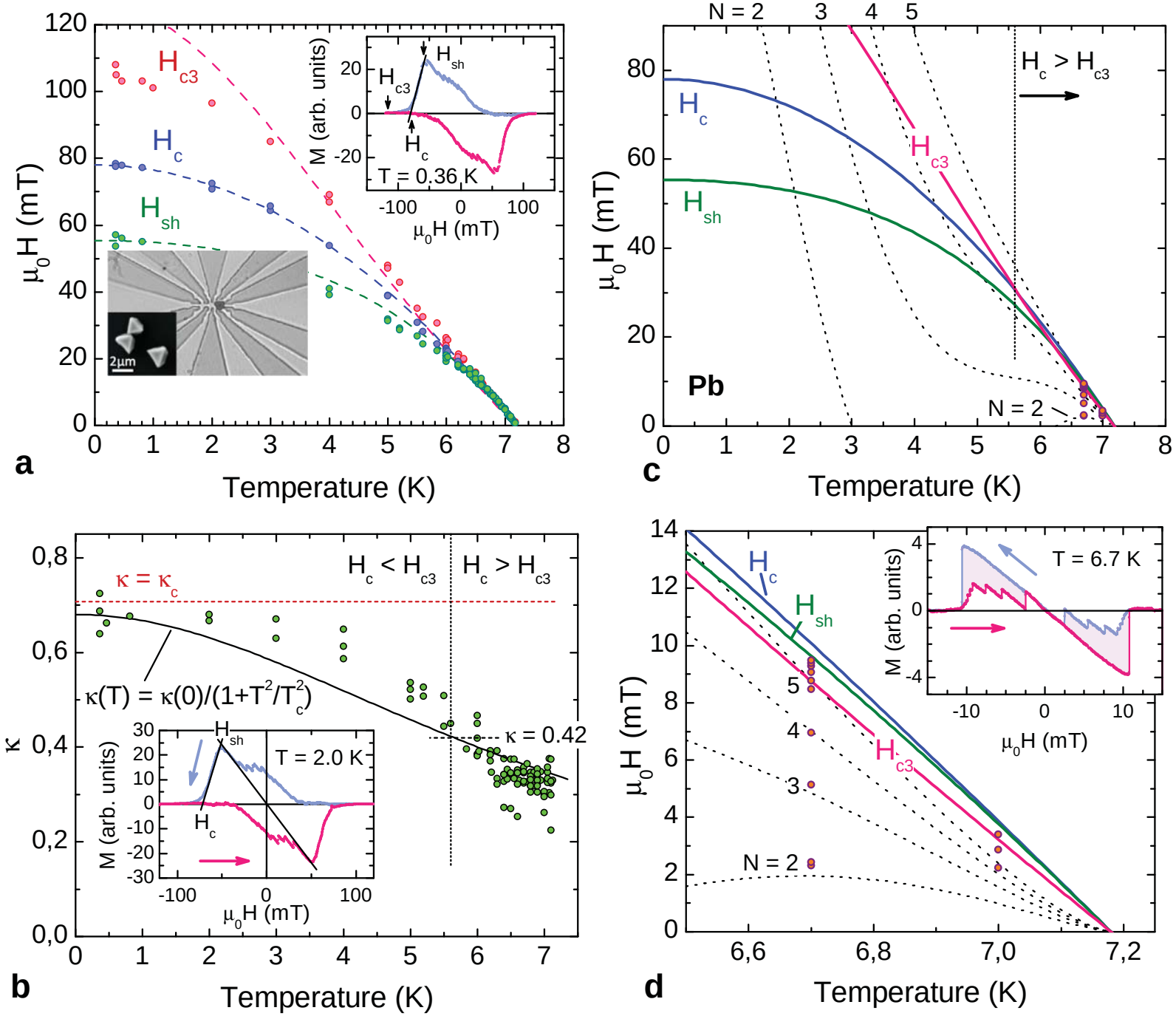
a
$\mu_0 H$ (mT)
Temperature (K)
H_{c3}
H_c
H_{sh}
M (arb. units)
T = 0.36 K
$\mu_0 H$ (mT)
2μm
b
$\kappa = \kappa_c$
$H_c < H_{c3}$
$H_c > H_{c3}$
$\kappa(T) = \kappa(0)/(1+T^2/T_c^2)$
$\kappa = 0.42$
κ
T = 2.0 K
c
N = 2
3
4
5
$H_c > H_{c3}$
Pb
d
T = 6.7 K
5
4
3
N = 2

Figure 4

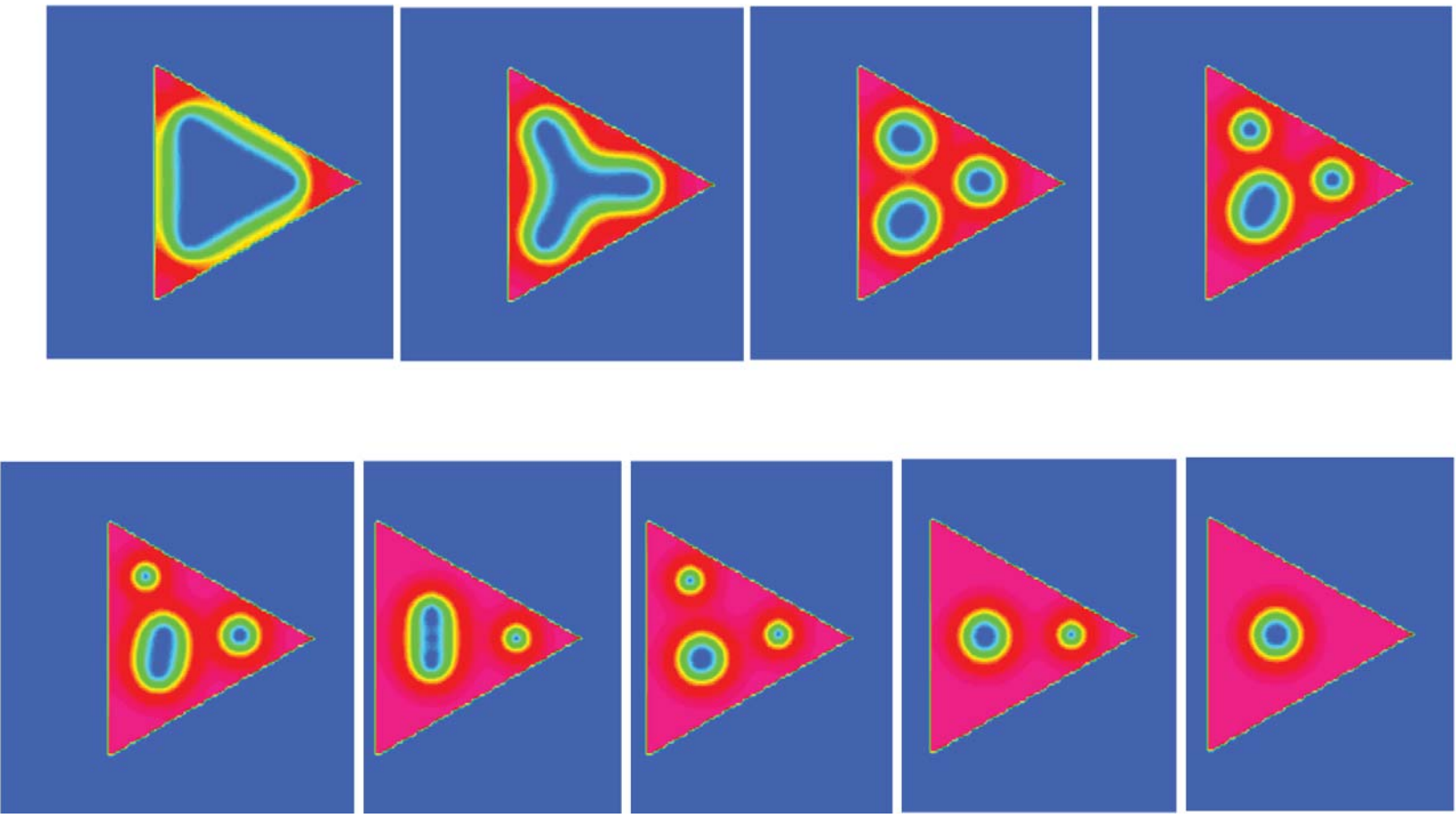

Figure 5

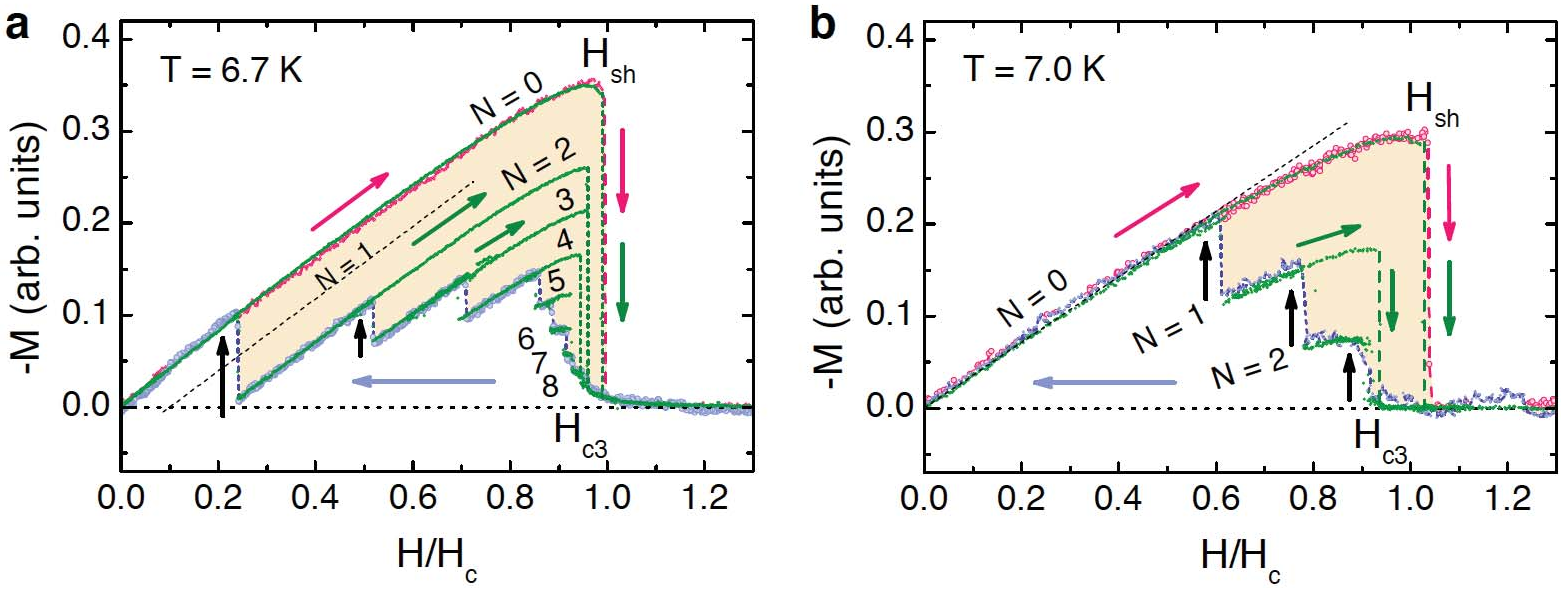
a
T = 6.7 K
H_sh
N = 0
N = 2
N = 1
3
4
5
6
7
8
H_c3
-M (arb. units)
H/H_c
0.0
0.1
0.2
0.3
0.4
0.0
0.2
0.4
0.6
0.8
1.0
1.2
b
T = 7.0 K
H_sh
N = 0
N = 1
N = 2
H_c3
-M (arb. units)
H/H_c